Engineering of a red-light–activated human cAMP/cGMP-specific phosphodiesterase

Carlos Gasser[a], Sandra Taiber[b], Chen-Min Yeh[c], Charlotte Helene Wittig[a], Peter Hegemann[d], Soojin Ryu[c], Frank Wunder[b], and Andreas Möglich[a,1]

[a]Biophysikalische Chemie and [d]Experimentelle Biophysik, Institut für Biologie, Humboldt-Universität zu Berlin, 10115 Berlin, Germany; [b]Lead Discovery, Bayer Pharma AG, 42096 Wuppertal, Germany; and [c]Developmental Genetics of the Nervous System, Max Planck Institute for Medical Research, 69120 Heidelberg, Germany

Edited by Loren L. Looger, Howard Hughes Medical Institute, Janelia Farm Campus, Ashburn, VA, and accepted by the Editorial Board May 8, 2014 (received for review November 19, 2013)

Sensory photoreceptors elicit vital physiological adaptations in response to incident light. As light-regulated actuators, photoreceptors underpin optogenetics, which denotes the noninvasive, reversible, and spatiotemporally precise perturbation by light of living cells and organisms. Of particular versatility, naturally occurring photoactivated adenylate cyclases promote the synthesis of the second messenger cAMP under blue light. Here, we have engineered a light-activated phosphodiesterase (LAPD) with complementary light sensitivity and catalytic activity by recombining the photosensor module of *Deinococcus radiodurans* bacterial phytochrome with the effector module of *Homo sapiens* phosphodiesterase 2A. Upon red-light absorption, LAPD up-regulates hydrolysis of cAMP and cGMP by up to sixfold, whereas far-red light can be used to down-regulate activity. LAPD also mediates light-activated cAMP and cGMP hydrolysis in eukaryotic cell cultures and in zebrafish embryos; crucially, the biliverdin chromophore of LAPD is available endogenously and does not need to be provided exogenously. LAPD thus establishes a new optogenetic modality that permits light control over diverse cAMP/cGMP-mediated physiological processes. Because red light penetrates tissue more deeply than light of shorter wavelengths, LAPD appears particularly attractive for studies in living organisms.

Quantitative analysis of cellular signaling networks and metabolic pathways demands observation and perturbation of living cells with spatial and temporal resolution commensurate with biologically relevant length and time scales. Noninvasive, reversible, and spatiotemporally precise perturbation is provided by optogenetics, which employs genetic means to introduce photoreceptor proteins serving as light-regulated actuators to target loci (1). Photoreceptors are commonly of modular architecture, where photosensor modules (input) absorb light and regulate the biological activity of associated effector modules in response (output). In some photoreceptors (e.g., rhodopsins), both modules are integrated into a single protein domain. Certain rhodopsins that function as light-gated ion channels (2, 3) or light-driven ion pumps (4) are particularly powerful because they realize optogenetic control over a fundamental property of every living cell, namely, the voltage across biological membranes. Rivaling this versatility, photoactivated adenylate cyclases (PACs) (5–7) catalyze the formation of cAMP in a blue-light–activated manner. Both cAMP and the related cGMP serve as ubiquitous second messengers in various responses in diverse organisms, including apoptosis, smooth muscle relaxation, and vision (8–11). Intracellular levels of cAMP and cGMP are tightly controlled by nucleotidyl cyclases and phosphodiesterases (PDEs)that catalyze the making and breaking of these second messengers (8–10). Although certain PDEs are involved in human vision (e.g., PDE6), no cAMP/cGMP-specific PDE is known that is directly regulated by light. Rather, in the PDE superfamily, N-terminal chemosensor modules of variable composition regulate the catalytic activity of a C-terminal effector module (8–10). In PDE2, PDE5, PDE6, PDE10, and PDE11, the sensor module consists of two cGMP PDE/adenylyl cyclase/FhlA (GAF) domains (12) that mediate regulation by cyclic nucleotides. Seminal work showed that the *Homo sapiens* cAMP/cGMP-specific PDE2A (*Hs*PDE2A) adopts a parallel homodimeric structure with the dyad interface formed by an extended α-helical spine (13) (Fig. 1*A*). Two GAF domains, denoted GAF-A and GAF-B, attach laterally to this spine and are tethered to the C-terminal PDE effector module by a coiled coil. Binding of cGMP to GAF-B induces fourfold allosteric activation of *Hs*PDE2A (13).

Strikingly similar overall architecture is observed for bacterial phytochrome (BPhy) red-light receptors (14–16) [e.g., in the dimeric photosensor module of *Pseudomonas aeruginosa* BPhy (*Pa*BPhy) (17)] (Fig. 1*A*). Highly reminiscent of *Hs*PDE2A, a trio of Per-ARNT-Sim (PAS) (18), GAF, and phytochrome (PHY)-specific domains are arranged laterally of a central α-helical spine. The histidine-kinase effector of *Pa*BPhy is not structurally resolved but is assumed to C-terminally connect to and communicate with the photosensor via a continuous coiled coil (17). A linear tetrapyrrole (bilin) chromophore, biliverdin in *Pa*BPhy, is covalently attached to a cysteine residue and is embedded in the GAF domain. The photocycle of all phytochromes comprises two (meta)stable states that differ in the conformation of the C15 = C16 double bond between rings C and D of the bilin chromophore (15, 16) (Fig. 1*B*). Typically, the 15*Z* isomer gives rise to a red-light–absorbing state denoted Pr, and the 15*E* isomer gives rise to a far-red-light–absorbing state denoted Pfr. Irradiation with red light (~650–700 nm) and far-red light (~700–750 nm) drives the fully reversible Pr→Pfr

Significance

Sensory photoreceptors not only enable organisms to derive spatial and temporal cues from incident light but also provide the basis for optogenetics, which denotes the manipulation by light of living systems with supreme spatial and temporal resolution. To expand the scope of optogenetics, we have engineered the light-activated phosphodiesterase LAPD, which degrades the ubiquitous second messengers cAMP and cGMP in a red-light–stimulated manner. Both cAMP and cGMP are key to the regulation of manifold physiological responses, and LAPD now augurs red-light control over these processes. As we demonstrate for two eukaryotic systems, LAPD does not require any additional exogenous factors, and thus permits the light perturbation of living cells in hitherto unrealized ways.

Author contributions: C.G., S.R., F.W., and A.M. designed research; C.G., S.T., C.-M.Y., and C.H.W. performed research; C.G., S.T., C.-M.Y., C.H.W., P.H., S.R., F.W., and A.M. analyzed data; and C.G. and A.M. wrote the paper.

The authors declare no conflict of interest.

This article is a PNAS Direct Submission. L.L.L. is a guest editor invited by the Editorial Board.

[1]To whom correspondence should be addressed. E-mail: andreas.moeglich@hu-berlin.de.

This article contains supporting information online at www.pnas.org/lookup/suppl/doi:10.1073/pnas.1321600111/-/DCSupplemental.

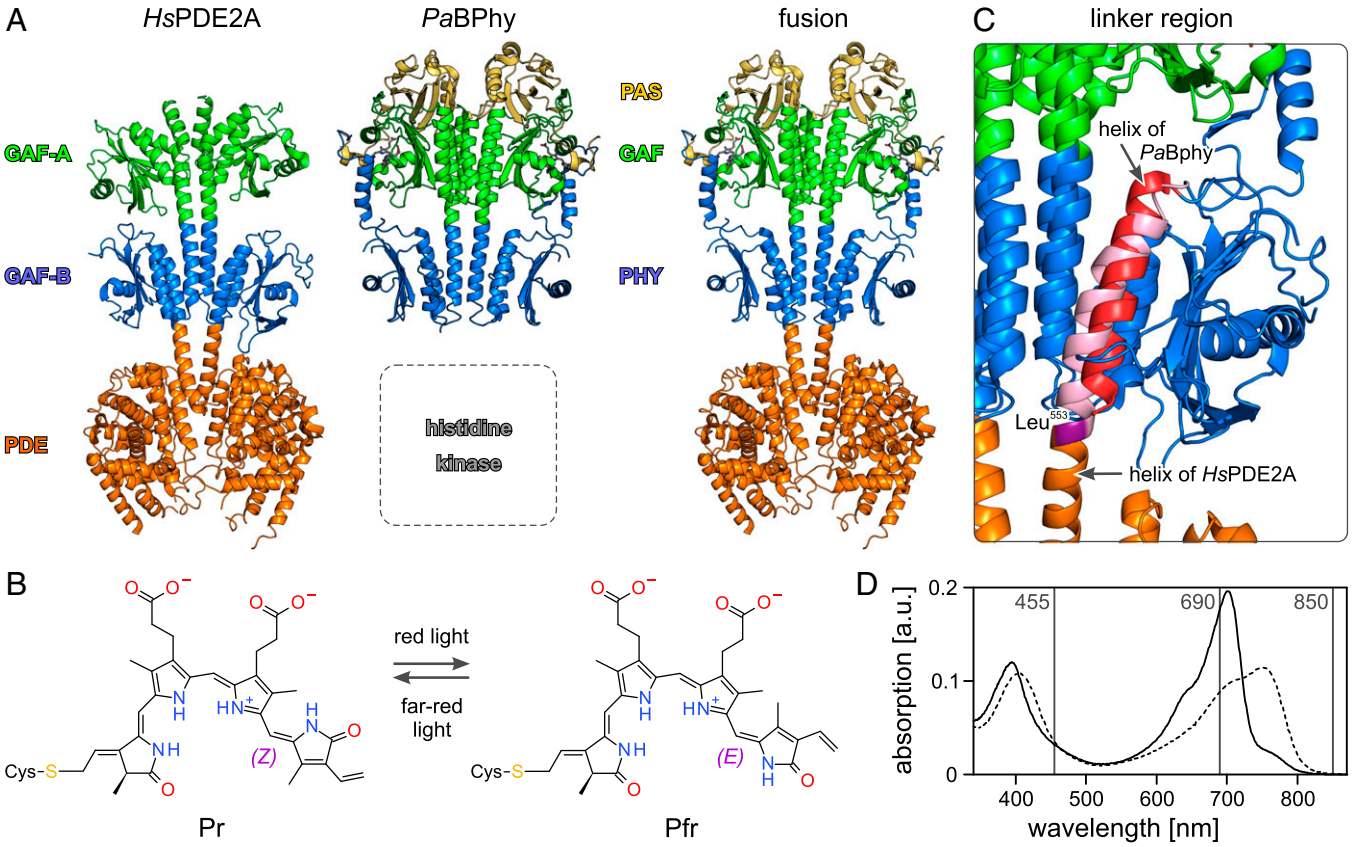

Fig. 1. Engineering of the red-light–activated PDE LAPD. (*A*) Both *Hs*PDE2A [*Left*, Protein Data Bank (PDB) ID code 3IBJ] and *Pa*BPhy (*Center*, PDB ID code 3C2W) adopt dimeric structures with extended α-helical interfaces; the regulatory GAF-A and GAF-B domains in PDE2A correspond structurally to the GAF and PHY domains of BPhy. (*Right*) Chimeric PDEs, shown as a model, derive their regulatory PAS-GAF-PHY tandem from BPhy and their catalytic domain from PDE2A. (*B*) The biliverdin chromophore of BPhys undergoes photoisomerization around the C15 = C16 double bond. The 15*Z* isomer gives rise to the red-light–absorbing state Pr, and the 15*E* isomer gives rise to the far-red-light–absorbing Pfr state. (*C*) Structures of *Hs*PDE2A and *Pa*BPhy were superposed with respect to their GAF-B and PHY domains, respectively. A helix emanating from the C terminus of the *Pa*BPhy PHY domain (red) spatially overlaps with a helix emanating from the N terminus of the *Hs*PDE2A catalytic domain (light pink). The residue leucine 553 at which the PDE domain is fused to the PAS-GAF-PHY photosensor in LAPD+2 is highlighted in deep purple. (*D*) Absorption spectra of LAPD in its dark-adapted (black line) and red-light–adapted (dashed line) states. Vertical lines indicate peak wavelengths of light sources used in this study. a.u., absorption units.

and Pfr→Pr transitions, respectively. Crucially, the Pr and Pfr states differ in the activity of the associated effector module; hence, a link between photochemistry and downstream responses is established. In conventional BPhys, such as the one from *Deinococcus radiodurans* (*Dr*BPhy) (19, 20), the Pr state is thermodynamically more stable and predominates in darkness; by contrast, *Pa*BPhy belongs to the bathyphytochromes, where the Pfr state is more stable.

Intrigued by the structural correspondence between the chemosensor of *Hs*PDE2A and the photosensor of BPhys, we wondered whether these modules are functionally interchangeable (21). Implementing this concept, we have engineered a light-activated phosphodiesterase (LAPD) that hydrolyzes cAMP and cGMP in a red-light–activated manner. Because LAPD also affords light control over the hydrolysis of cyclic nucleotides in eukaryotic cell culture and whole animals, the optogenetic arsenal is expanded by a new functionality.

Results

Structure-Guided Engineering of LAPD. Structural superposition of *Hs*PDE2A and the PAS-GAF-PHY tandem of *Pa*BPhy provides a rationale for how chimeras between the two parent proteins should be constructed (Fig. 1*A*). In particular, helices emanating from the C terminus of the *Pa*BPhy PHY domain can be spatially overlapped with helices emanating from the N terminus of the *Hs*PDE2A catalytic domain (Fig. 1*C*). Because expression of chimeras between *Hs*PDE2A and *Pa*BPhy failed to yield soluble protein, we switched to using *Dr*BPhy, for which the structures of the PAS and GAF domains have been elucidated (20). Initially, we generated a chimeric construct, denoted LAPD+2, that connects the PAS-GAF-PHY domains of *Dr*BPhy (amino acids 1–506) to the PDE domain of *Hs*PDE2A (amino acids 553–941) (Fig. S1 and Table S1). The chimeric protein was expressed in *Escherichia coli* together with heme oxygenase, which supplies the biliverdin chromophore (22). Upon purification, we found that LAPD+2 possesses no appreciable catalytic activity, regardless of illumination. Spurred by previous findings that the length of the linker between sensor and effector modules strongly affects catalytic activity and regulation of signal receptors (23, 24), we generated chimeras between *Dr*BPhy and *Hs*PDE2A that differ in the length of this linker (Fig. S1 and Table S1). In particular, a deletion of two residues [*Dr*BPhy (amino acids 1–506) linked to *Hs*PDE2A (amino acids 555–941)] yielded a construct exhibiting light-regulated cyclic nucleotide hydrolysis (compare below); hence, we refer to this construct as LAPD. LAPD autonomously incorporates its biliverdin chromophore and undergoes the same characteristic Pr↔Pfr photochemistry as the parent protein *Dr*BPhy (Fig. 1*D*). Using absorption spectroscopy, we determined the amount of apoprotein lacking biliverdin to be below 3 ± 5%.

Red-Light–Activated PDE Activity of LAPD. We measured cGMP and cAMP hydrolysis catalyzed by LAPD in its dark-adapted state and in its red-light–adapted state following illumination with 690-nm light. Reactions were initiated by addition of cyclic nucleotides, and aliquots taken at specific times were analyzed by reverse-phase HPLC. As exemplified for red-light–adapted LAPD at 100 μM cGMP, the HPLC elution profile shows substrate (cGMP) depletion and concomitant product (GMP) formation progressing with reaction time (Fig. 2*A*). Integration of the peak areas allowed the determination of initial reaction velocities, v_0, and revealed that catalytic turnover of LAPD is enhanced under red light compared with dark conditions (Fig. 2*B* and Fig. S2). LAPD followed Michaelis–Menten kinetics for cGMP hydrolysis under both dark and red-light conditions (Fig. 2*C*). When normalized to the amount of LAPD, maximum reaction velocities at substrate saturation, v_{max}, of 2.5 ± 0.4 μM·min^{-1} (nM LAPD)$^{-1}$ and 15.1 ± 0.3 μM·min^{-1} (nM LAPD)$^{-1}$ were obtained in the dark and under 690-nm light, respectively, corresponding to a sixfold enhancement upon light exposure. By contrast, substrate affinity was largely unaffected by illumination with K_m(cGMP) amounting to 440 ± 140 μM in the dark and to 340 ± 20 μM in red light. For the parent enzyme *Hs*PDE2A (13), cGMP binding to GAF-B allosterically activates by about fourfold, yielding v_{max} = 2.5 ± 0.9 μM·min^{-1} (nM enzyme)$^{-1}$, which is closely similar to dark-adapted LAPD. However, *Hs*PDE2A showed higher affinity for the substrate cGMP [K_m(cGMP) = 78 ± 5 μM].

As is true for *Hs*PDE2A, LAPD has dual specificity and also catalyzes the hydrolysis of cAMP with a v_{max} of 1.8 ± 0.3 μM·min^{-1} (nM LAPD)$^{-1}$ in the dark and 6.5 ± 0.2 μM·min^{-1} (nM LAPD)$^{-1}$ under 690-nm light, corresponding to a fourfold enhancement in the light (Fig. S3). Affinity for cAMP amounted to 470 ± 170 μM under dark conditions and to 180 ± 20 μM under 690-nm light. For comparison, PDE2A prepared from bovine heart is allosterically activated five- to sixfold by cGMP and hydrolyzes cAMP with v_{max} = 12.4 μM·min^{-1} (nM enzyme)$^{-1}$ and K_m(cAMP) ≈ 30 μM (25).

To assess the influence of different light qualities on LAPD activity, we conducted hydrolysis experiments at 1 mM cGMP substrate concentration, where 690-nm light induces an approximately sevenfold enhancement of turnover relative to dark (Fig. 2*D*). For far-red illumination, we resorted to an 850-nm light-emitting diode (LED) whose emission maximum is well in the IR range. Irradiation with 850-nm light led to a reproducible 20% increase of LAPD activity (two-tailed Welch's *t* test, P = 0.03), which we attribute to residual absorption of dark-adapted LAPD at wavelengths contained in the LED emission spectrum (Fig. 2*D*). Application of 690-nm light following 850-nm light results in full activation of LAPD. To test whether red-light–induced activation of LAPD can be reverted by irradiation with far-red light, we first exposed LAPD to saturating 690-nm light before applying 850-nm light. With increasing duration of 850-nm irradiation, LAPD activity decreased; 850-nm light apparently drives the reverse transition, Pfr→Pr, and can be used to attenuate LAPD activity (Fig. 2*D*). Although the kinetics for this transition are slow, the observed effect is not merely due to thermal reversion of the Pfr to the Pr state during illumination with 850-nm light, which only accounts for a small fraction of the loss in LAPD activity (Fig. 2*D*). Due to its Soret absorption at around 400 nm (compare Fig. 1*D*), LAPD can also be photoactivated to full extent by blue light (455 nm) and broadband white light (Fig. 2*D*).

Although the LAPD protein prepared by heterologous expression in *E. coli* incorporated its biliverdin chromophore to near-full extent, the efficiency of incorporation might be different in other settings, particularly in vivo (compare below). To assess the activity of apo-LAPD, we generated the C24A mutant of LAPD in which the cysteine residue necessary for covalent chromophore attachment has been removed. Absorption spectroscopy confirms that LAPD C24A is devoid of chromophore, and thus represents a valid proxy for apo-LAPD.

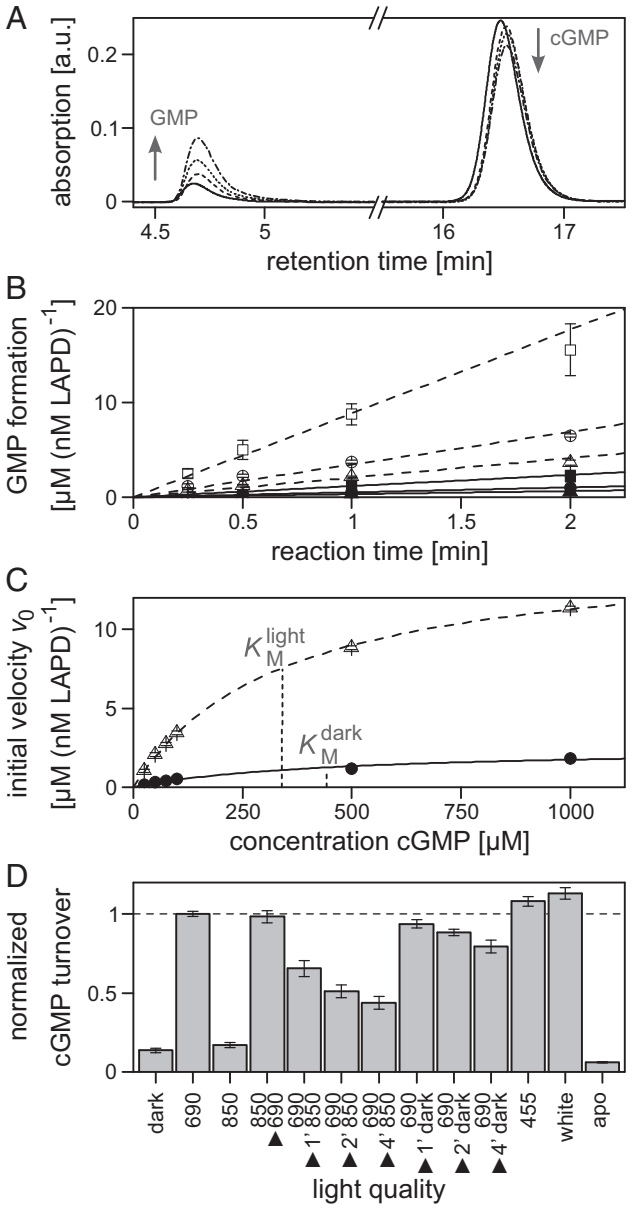

Fig. 2. Red-light–activated cGMP hydrolysis by LAPD. (*A*) Aliquots were taken from a reaction mix containing 5 nM red-light–adapted LAPD and 100 μM cGMP after 15 s (solid line), 30 s (dashed line), 60 s (dotted line), and 120 s (dashed/dotted line), and were analyzed by HPLC. Over time, the cGMP peak decreases and the GMP peak concomitantly increases (arrows). (*B*) Integration of peak areas from HPLC analysis yields initial reaction velocities, v_0, at concentrations of 50 μM (▲), 100 μM (●), and 500 μM (■) cGMP. LAPD activity is enhanced under 690-nm light (open symbols) compared with dark conditions (closed symbols). Data are mean ± SD of two measurements; lines denote linear fits to determine initial v_0 values. (*C*) LAPD displays Michaelis–Menten kinetics in both darkness (●, solid line) and under 690-nm light (Δ, dashed line). The v_0 values were determined by least-squares fitting and are reported as mean ± asymptotic SE. The v_{max} is increased from 2.5 ± 0.4 μM·min^{-1} (nM LAPD)$^{-1}$ in the dark to 15.1 ± 0.3 μM·min^{-1} (nM LAPD)$^{-1}$ under 690-nm light; the K_m values amount to 440 ± 140 μM in the dark and to 340 ± 20 μM under 690-nm light. Lines denote fits to hyperbolic functions. (*D*) Influence of different light qualities on LAPD activity was studied at an initial cGMP concentration of 1 mM. LAPD was subjected to different light regimes: dark; 690-nm light; 850-nm light; 850-nm light followed by 690-nm light; 690-nm light followed by 850-nm light for 1, 2, and 4 min; 690-nm light followed by dark incubation for 1, 2, and 4 min; 455-nm light; and broadband white light. The rightmost column (apo) represents the activity of LAPD C24A, which lacks the biliverdin chromophore. Catalytic turnover was normalized to the value obtained for 690-nm light. Data are mean ± SD of four measurements.

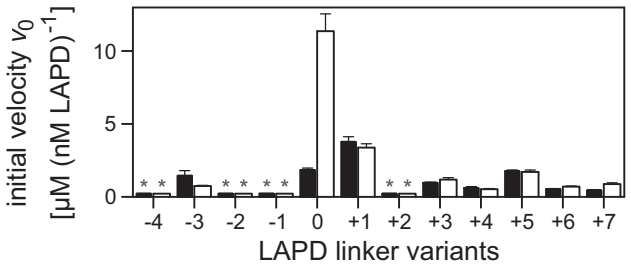

Fig. 3. Linker-length dependence of catalytic activity and light regulation in LAPD. Initial reaction velocities in the dark (black bars) or under 690-nm light (white bars) at 1 mM cGMP for LAPD variants differing in the length of the linker between the photosensor and effector modules. Data were determined by least-squares fitting and are reported as mean ± asymptotic SE; asterisks denote activities below the detection limit.

Hydrolysis experiments at 1 mM cGMP concentration reveal that the specific activity of LAPD C24A amounts to 43.7 ± 5.6% of holo-LAPD in its dark-adapted, low-activity state (Fig. 2*D*).

Linker Composition Governs Enzymatic Activity and Regulation by Light. Studies on chimeric adenylate cyclases (23) and blue-light–regulated histidine kinases (24) revealed that the length of α-helical linkers between sensor and effector modules crucially governs the activity and signal response of the composite receptors. To probe whether these mechanistic principles extend to LAPD, we generated a series of insertion variants, denoted LAPD+1 through LAPD+7, in which up to seven consecutive residues were inserted into the LAPD linker, and a series of deletion variants, denoted LAPD−1 through LAPD−4, in which up to four consecutive residues were removed (Fig. S1 and Table S1). All variants could be expressed and purified; all constructs incorporated biliverdin to a similar or slightly lower extent as LAPD and showed reversible Pr↔Pfr photochemistry. Measurements of cGMP hydrolysis at 1 mM substrate concentration under dark and red-light conditions (690 nm) revealed that none of the LAPD derivatives were regulated by red light to a significant extent, and most of them showed only basal or even no detectable enzymatic activity (Fig. 3). However, LAPD+1 had constitutive activity at an intermediate level between dark-adapted and red-light–adapted LAPD. Apparently, LAPD possesses an optimized geometry, and the presently tested deviations in linker length strongly impair enzymatic activity and light regulation.

LAPD Displays Light-Regulated Activity in Eukaryotic Cells. After ascertaining red-light–activated enzymatic activity of LAPD in vitro, we examined whether LAPD can modulate intracellular cyclic nucleotide levels in CHO cell culture (Fig. 4) and in zebrafish (Fig. 5).

We stably expressed LAPD in a cGMP-reporter CHO cell line used previously for the characterization of the cellular activity of PDE2-specific inhibitors (26, 27). Briefly, this cell line stably expresses a receptor for the atrial natriuretic peptide (ANP), the cyclic nucleotide–gated ion channel CNGA2, and the luminescent reporter aequorin (Fig. S4*A*). Upon ANP stimulation, the receptor catalyzes the production of intracellular cGMP, which, in turn, triggers opening of CNGA2 channels; resultant influx of calcium and subsequent binding by aequorin stimulate an increase of bioluminescence. When functionally expressed in these cells, LAPD would catalyze the breakdown of cGMP, thus resulting in decreased luminescence.

In the dark, ANP addition induced a concentration-dependent increase of bioluminescence in the LAPD reporter cell line with an apparent EC_{50} ANP dose of 1.2 ± 0.1 nM, which is close to the reported EC_{50} value of 0.8 nM for ANP receptor stimulation (28) (Fig. 4*A*). When exposed to white light, ANP stimulation also led to a concentration-dependent increase of bioluminescence (EC_{50} = 3.9 ± 1.0 nM), but luminescence maximally reached 20–35% of the value under dark conditions, indicating light-induced PDE activity. Note that reporter luminescence is governed by multiple nonlinear processes; hence, we attribute the slightly higher EC_{50} value in the light to increased LAPD activity as opposed to altered ANP receptor affinity. Interestingly, the endogenous amount of biliverdin present in CHO cells suffices to support the maximal light response, because incubation with exogenously added biliverdin had no effect on light-regulated PDE activity. To further pinpoint the observed light effect to LAPD, we titrated the LAPD reporter cell line with the PDE2-specific inhibitor BAY 60-7550 (Axxora Life Sciences, Inc.) (26) and stimulated cGMP production by addition of 10 nM ANP (Fig. 4*B*). At BAY 60-7550 concentrations above 20 nM, LAPD is completely inhibited and bioluminescence under dark and light conditions is virtually indistinguishable. The EC_{50} dose of 3.0 ± 0.2 nM determined under light conditions is closely similar to the value of 6 nM for WT *Hs*PDE2A (26). Control cell lines expressing *Hs*PDE2A instead of LAPD did not respond to light (Fig. S4*B*).

In a second line of experiments, we expressed LAPD in zebrafish embryos and measured whole-body cAMP levels under different light conditions (Fig. 5). Embryos were injected at the one-cell stage with LAPD RNA. At 1 d postfertilization, the embryos were treated with forskolin to increase intracellular cAMP substrate levels (29) and were incubated for 5 h under red light or under IR light. Animals were then killed, and whole-body cAMP levels were determined by ELISA. Under red light, cAMP levels were suppressed by around 40% in LAPD-injected embryos relative to uninjected control embryos (two-tailed Welch's *t* test, $P < 10^{-5}$) (Fig. 5*A*). By contrast, under IR light, no significant difference in cAMP levels between LAPD-injected and uninjected control embryos was observed ($P = 0.81$) (Fig. 5*B*). As in the experiments using CHO cells, red-light enhancement of LAPD activity did not require exogenous biliverdin addition.

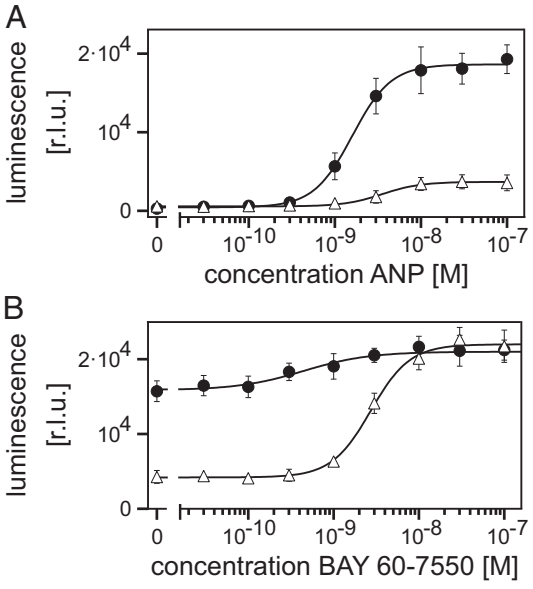

Fig. 4. LAPD mediates light-activated cGMP hydrolysis in CHO cells. (*A*) LAPD reporter cell line was stimulated with different amounts of ANP in the dark (●) or light (Δ). The luminescence signal in the light is suppressed compared with the dark. Luminescence data are reported as relative light units (r.l.u.) and represent mean ± SEM of six to seven measurements; lines denote fits to hyperbolic functions. (*B*) Addition of the PDE2 inhibitor BAY 60-7550 specifically inhibits the catalytic activity of LAPD under both dark and light conditions. Data are mean ± SEM of six to seven measurements; lines denote fits to hyperbolic functions.

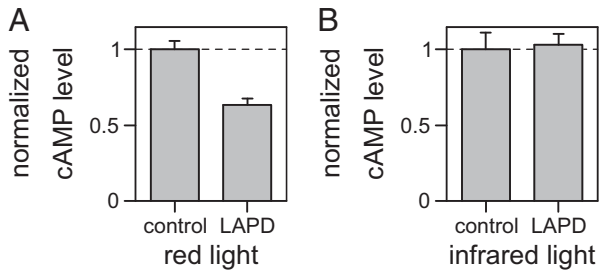

Fig. 5. LAPD mediates light-activated cAMP hydrolysis in zebrafish embryos. Zebrafish embryos were injected at the one-cell stage. At 1 d postfertilization, embryos were incubated with forskolin and illuminated with red or IR light; whole-body cAMP levels were then determined by ELISA. (*A*) Under red light, LAPD expression resulted in suppression of cAMP levels by 40% in comparison to uninjected control embryos (two-tailed Welch's *t* test, $P < 10^{-5}$). Data are mean ± SEM of 23 LAPD-injected and 22 uninjected cohorts, where each cohort comprised 15 individual embryos. (*B*) Under IR light, cAMP levels are the same in LAPD-injected and uninjected control embryos. Data are mean ± SEM of 16 cohorts each.

Taken together, these results show that LAPD can be functionally expressed in eukaryotic cell cultures and in whole animals, can be activated by light exposure, does not demand exogenous addition of biliverdin, and may be specifically inhibited by BAY 60-7550.

Discussion

Commutability of Sensor and Effector Modules in Signal Receptors. The successful engineering of LAPD unequivocally shows that fundamental principles and mechanisms are shared across certain signal receptors, and that the constituent sensor and effector modules of these receptors are hence functionally interchangeable. Evidently, modular commutability spans signal receptors that harbor disparate (enzymatic) activities (e.g., histidine kinases vs. PDEs) that respond to completely different signals (e.g., red light vs. secondary metabolites) and are of utterly different provenance (e.g., prokaryotic vs. eukaryotic). The remarkable versatility of the underlying signal transduction mechanisms is further borne out in work on chimeras between mammalian cGMP-activated PDEs and cyanobacterial cAMP-activated adenylate cyclases (30, 31). By exchanging the GAF sensor modules, the stimulus response of the adenylate cyclase could be reprogrammed from cAMP to cGMP, but, in contrast to LAPD, catalytic activity was severely impaired. Our work now extends the commutability principle from cyclic nucleotide–regulated chemoreceptors to red-light–regulated photoreceptors, thus providing clear-cut avenues for the engineering of novel receptors [e.g., red-light–regulated adenylate cyclases, as recently demonstrated by Gomelsky and Ryu (32)].

Interestingly, the structural superposition between *Pa*BPhy and *Hs*PDE2A (compare Fig. 1 *A* and *C*) favored the chimeric construct LAPD+2, which had no appreciable PDE activity, however. Only after deletion of two residues from the linker did we obtain the LAPD construct with PDE activity that was light-regulated. Although the reason for this discrepancy is unclear, a two-residue deletion might induce torsional strain in the coiled-coil linker required for light regulation of PDE activity. For the parent receptor *Hs*PDE2A, signal transduction was proposed to involve signal-dependent rearrangements of the interface between the two catalytic PDE subunits (13, 33). In the absence of signal, a low-activity state is assumed, where the two PDE subunits are spatially arranged such that their substrate-binding pockets are occluded by a protein loop, denoted the H-loop. In the presence of signal (cGMP in the case of *Hs*PDE2A), a high-activity state is assumed, where reorientation of the PDE domains leads to displacement of the H-loop and concomitant exposure of the substrate-binding pocket (13). The observation that the majority of all LAPD linker variants have constitutively low PDE activity (compare Fig. 3) now suggests that the low-activity state of PDE2A is thermodynamically preferred; free energy must be invested to convert the PDE to the high-activity state (e.g., via cGMP binding to GAF-B in the case of *Hs*PDE2A or via light absorption in the case of LAPD).

At first glance, it seems a conundrum that disparate sensors and effectors can so readily communicate. An elegant solution to this problem is outlined in a recent essay (33). Effectors intrinsically exist in equilibrium between states of low activity and high activity, which we identify as T (tense) and R (relaxed) states, respectively (21, 34, 35). Quaternary structural transitions in dimeric signal receptors as discussed for *Hs*PDE2A (compare above) are apparently key in repositioning catalytic units to allow adoption of their high-activity state (9, 33). Crucially, the sensor module merely shifts the intrinsic equilibrium between T and R states in a signal-dependent manner but does not alter the states per se. α-helical coiled coils recur as linkers in signal receptors, arguably because they do not demand direct contacts between sensors and effectors, and they are hence well suited to transmit signals over extended molecular distances (e.g., across biological membranes) (36). Signal transduction could involve different types of helical motions (e.g., rotation, dissociation, piston and pivot) (33); notably, for HAMP domains (histidine kinases, adenylate cyclases, methyl-accepting proteins, and phosphatases) (37) and sensor histidine kinases (24), which often occur in conjunction with GAF domains, signal-induced rotary movements of coiled-coil helices were invoked.

LAPD as an Orthogonal Optogenetic Tool. In LAPD, we have established a novel optogenetic modality that achieves light-controlled perturbation of living cells in hitherto unrealized ways. As we demonstrate, LAPD enhances the hydrolysis of cyclic nucleotide second messengers in eukaryotic cells upon light exposure. Of key advantage, the biliverdin chromophore of LAPD is apparently available intracellularly in sufficient quantities, thus obviating the need for exogenous addition and enabling true genetic encoding. This contrasts with the initial application of a photochemically impaired *Dr*BPhy photosensor module in mouse liver as a near-IR fluorescent probe (38); fluorescence could be markedly enhanced by exogenous addition of biliverdin, which indicates that for this application and in these cells, the endogenous level of biliverdin was below saturation. However, improved fluorescent BPhys no longer require exogenous biliverdin addition (39), indicating that not only the bioavailability of the chromophore but also the efficiency of its incorporation matters. Both cAMP and cGMP are involved in the regulation of manifold biological processes as diverse as the stress response in zebrafish (40), parasite infectivity (41), and *Drosophila* behavior (7), and LAPD augurs optogenetic control over these processes. Notably, red and far-red light penetrate tissue much more deeply than light of shorter wavelengths, thus making LAPD particularly well suited for optogenetic studies on whole animals (compare Fig. 5); however, it remains to be further corroborated whether the chromophore biliverdin is readily available in all tissues and cell types. Of particular advantage, the specific activity of apo-LAPD is around 2.3-fold lower than that of holo-LAPD in its low-activity, dark-adapted state (compare Fig. 2*D*); consequently, relatively large light effects could still be induced even in the presence of significant levels of apoprotein. Our data show that red light enhances LAPD activity by a factor of sixfold, whereas the complementary blue-light–activated adenylate cyclases exhibit activation factors that can be more than one order of magnitude higher (5–7). However, the light induction factor of LAPD is virtually the same as for cGMP activation of the parent receptor *Hs*PDE2A, implying that meaningful physiological effects could still be elicited. Furthermore, with the basic design rule for red-light–regulated PDEs now established, other variants with different, possibly improved properties can readily be engineered [e.g., by introducing mutations that modulate Pr↔Pfr photochemistry (42), by resorting to BPhys with favorable characteristics (43), by replacing the effector with other PDE domains].

More generally, LAPD exemplifies that not only plant phytochromes (44) but also bacterial phytochromes constitute powerful building blocks in the engineering of novel optogenetic actuators (45). Although the precise mechanism of signal transduction is fully understood neither for BPhys nor for PDEs, coiled-coil linkers between photosensor and effector moieties appear essential, as also observed for certain blue-light receptors (36). Engineering on the basis of BPhys is hence particularly applicable to homodimeric effector proteins. Coupling to a BPhy photosensor could constrain, and thus align, the constituent monomers of dimeric effectors in either productive or nonproductive orientations; light absorption could alter or relieve this constraint and allow the monomers to adopt a new orientation with different activity. Decisive advantages of phytochromes are reversible switching by two light colors, facilitating enhanced spatiotemporal resolution, and deeper tissue penetration of red light, facilitating optogenetics in thicker slices and live animals. In contrast to plant phytochromes, BPhys use the chromophore biliverdin, which apparently accrues as a natural degradation product of heme, and thus does not need to be added exogenously.

Materials and Methods

The LAPD+2 fusion construct was generated by restriction cloning and was ligated into pASK43; LAPD, the C24A mutant, and linker variants were generated by site-directed mutagenesis. For experiments in CHO cells and zebrafish, the LAPD gene was cloned into the pEGFP-N1 and pGEM vectors. LAPD expression was carried out in *E. coli* BL21(DE3) cells expressing *Synechocystis* sp. heme oxygenase 1. Protein was purified by immobilized metal ion affinity chromatography, and concentration was determined by absorption spectroscopy. Catalytic activity was measured in vitro at 25 °C in the dark or under illumination 2 min before and during the reaction. Reaction aliquots were analyzed by reverse-phase HPLC on a C18 column. Elution was monitored by absorbance, and peak areas were integrated to determine the amounts of substrate and product.

Stable LAPD reporter and control *Hs*PDE2A cell lines were generated by hygromycin selection (27). PDE activity was measured with cells incubated in the dark or under white light before measurement (26). Experiments performed in this study were conducted according to the German animal welfare law and were approved by the Animal Protection Office of the Max Planck Institute of Medical Research/University of Heidelberg. LAPD RNA was injected into embryos at the one-cell stage. After maintenance in the dark, embryos were dechorionated manually. Both uninjected control and LAPD-injected embryos were treated with 300 μM forskolin and illuminated with red or IR light. Whole-body cAMP levels were determined using an ELISA kit (Enzo Life Sciences).

ACKNOWLEDGMENTS. We thank F. Richter and the laboratory of A.M. for discussions; R. Arndt for LED devices; J. Pustogowa, M. Stierl, J. Wietek, and A. Woermann for excellent assistance; and T. Kohchi for pKT270. Funding was provided through a Sofja Kovalevskaya Award by the Alexander von Humboldt Foundation (to A.M.), by the Cluster of Excellence "Unifying Concepts in Catalysis" of the Deutsche Forschungsgemeinschaft (DFG) (to P.H. and A.M.), by DFG Grant FOR1279 (to P.H., S.R., and A.M.), and by the Max Planck Society (to S.R.).

1. Deisseroth K (2011) Optogenetics. *Nat Methods* 8(1):26–29.
2. Nagel G, et al. (2002) Channelrhodopsin-1: A light-gated proton channel in green algae. *Science* 296(5577):2395–2398.
3. Nagel G, et al. (2003) Channelrhodopsin-2, a directly light-gated cation-selective membrane channel. *Proc Natl Acad Sci USA* 100(24):13940–13945.
4. Zhang F, et al. (2007) Multimodal fast optical interrogation of neural circuitry. *Nature* 446(7136):633–639.
5. Schröder-Lang S, et al. (2007) Fast manipulation of cellular cAMP level by light in vivo. *Nat Methods* 4(1):39–42.
6. Ryu M-H, Moskvin OV, Siltberg-Liberles J, Gomelsky M (2010) Natural and engineered photoactivated nucleotidyl cyclases for optogenetic applications. *J Biol Chem* 285(53): 41501–41508.
7. Stierl M, et al. (2011) Light modulation of cellular cAMP by a small bacterial photoactivated adenylyl cyclase, bPAC, of the soil bacterium Beggiatoa. *J Biol Chem* 286(2): 1181–1188.
8. Francis SH, Blount MA, Corbin JD (2011) Mammalian cyclic nucleotide phosphodiesterases: Molecular mechanisms and physiological functions. *Physiol Rev* 91(2): 651–690.
9. Conti M, Beavo J (2007) Biochemistry and physiology of cyclic nucleotide phosphodiesterases: Essential components in cyclic nucleotide signaling. *Annu Rev Biochem* 76:481–511.
10. Omori K, Kotera J (2007) Overview of PDEs and their regulation. *Circ Res* 100(3): 309–327.
11. Gomelsky M (2011) cAMP, c-di-GMP, c-di-AMP and now cGMP: Bacteria use them all! *Mol Microbiol* 79(3):562–565.
12. Ho YS, Burden LM, Hurley JH (2000) Structure of the GAF domain, a ubiquitous signaling motif and a new class of cyclic GMP receptor. *EMBO J* 19(20):5288–5299.
13. Pandit J, Forman MD, Fennell KF, Dillman KS, Menniti FS (2009) Mechanism for the allosteric regulation of phosphodiesterase 2A deduced from the X-ray structure of a near full-length construct. *Proc Natl Acad Sci USA* 106(43):18225–18230.
14. Hughes J, et al. (1997) A prokaryotic phytochrome. *Nature* 386(6626):663.
15. Rockwell NC, Su YS, Lagarias JC (2006) Phytochrome structure and signaling mechanisms. *Annu Rev Plant Biol* 57:837–858.
16. Hughes J (2013) Phytochrome cytoplasmic signaling. *Annu Rev Plant Biol* 64:377–402.
17. Yang X, Kuk J, Moffat K (2008) Crystal structure of Pseudomonas aeruginosa bacteriophytochrome: Photoconversion and signal transduction. *Proc Natl Acad Sci USA* 105(38):14715–14720.
18. Taylor BL, Zhulin IB (1999) PAS domains: Internal sensors of oxygen, redox potential, and light. *Microbiol Mol Biol Rev* 63(2):479–506.
19. Bhoo SH, Davis SJ, Walker J, Karniol B, Vierstra RD (2001) Bacteriophytochromes are photochromic histidine kinases using a biliverdin chromophore. *Nature* 414(6865): 776–779.
20. Wagner JR, Brunzelle JS, Forest KT, Vierstra RD (2005) A light-sensing knot revealed by the structure of the chromophore-binding domain of phytochrome. *Nature* 438(7066):325–331.
21. Möglich A, Moffat K (2010) Engineered photoreceptors as novel optogenetic tools. *Photochem Photobiol Sci* 9(10):1286–1300.
22. Mukougawa K, Kanamoto H, Kobayashi T, Yokota A, Kohchi T (2006) Metabolic engineering to produce phytochromes with phytochromobilin, phycocyanobilin, or phycoerythrobilin chromophore in Escherichia coli. *FEBS Lett* 580(5):1333–1338.
23. Winkler K, Schultz A, Schultz JE (2012) The S-helix determines the signal in a Tsr receptor/adenylyl cyclase reporter. *J Biol Chem* 287(19):15479–15488.
24. Möglich A, Ayers RA, Moffat K (2009) Design and signaling mechanism of light-regulated histidine kinases. *J Mol Biol* 385(5):1433–1444.
25. Martins TJ, Mumby MC, Beavo JA (1982) Purification and characterization of a cyclic GMP-stimulated cyclic nucleotide phosphodiesterase from bovine tissues. *J Biol Chem* 257(4):1973–1979.
26. Wunder F, Gnoth MJ, Geerts A, Barufe D (2009) A novel PDE2A reporter cell line: Characterization of the cellular activity of PDE inhibitors. *Mol Pharm* 6(1):326–336.
27. Wunder F, Woermann A, Geerts A, Milde M (2013) Pharmacological characterization of receptor guanylyl cyclase reporter cell lines. *Eur J Pharmacol* 698(1-3):131–136.
28. Li B, et al. (1995) Minimization of a polypeptide hormone. *Science* 270(5242): 1657–1660.
29. Barresi MJ, Stickney HL, Devoto SH (2000) The zebrafish slow-muscle-omitted gene product is required for Hedgehog signal transduction and the development of slow muscle identity. *Development* 127(10):2189–2199.
30. Kanacher T, Schultz A, Linder JU, Schultz JE (2002) A GAF-domain-regulated adenylyl cyclase from Anabaena is a self-activating cAMP switch. *EMBO J* 21(14):3672–3680.
31. Bruder S, et al. (2005) The cyanobacterial tandem GAF domains from the cyaB2 adenylyl cyclase signal via both cAMP-binding sites. *Proc Natl Acad Sci USA* 102(8): 3088–3092.
32. Gomelsky M, Ryu M-H (2013) US Patent WO2013016693 A2.
33. Schultz JE, Natarajan J (2013) Regulated unfolding: A basic principle of intraprotein signaling in modular proteins. *Trends Biochem Sci* 38(11):538–545.
34. Möglich A, Ayers RA, Moffat K (2009) Structure and signaling mechanism of Per-ARNT-Sim domains. *Structure* 17(10):1282–1294.
35. Monod J, Wyman J, Changeux JP (1965) On the nature of allosteric transitions: A plausible model. *J Mol Biol* 12:88–118.
36. Diensthuber RP, Bommer M, Gleichmann T, Möglich A (2013) Full-length structure of a sensor histidine kinase pinpoints coaxial coiled coils as signal transducers and modulators. *Structure* 21(7):1127–1136.
37. Hulko M, et al. (2006) The HAMP domain structure implies helix rotation in transmembrane signaling. *Cell* 126(5):929–940.
38. Shu X, et al. (2009) Mammalian expression of infrared fluorescent proteins engineered from a bacterial phytochrome. *Science* 324(5928):804–807.
39. Filonov GS, et al. (2011) Bright and stable near-infrared fluorescent protein for in vivo imaging. *Nat Biotechnol* 29(8):757–761.
40. De Marco RJ, Groneberg AH, Yeh C-M, Castillo Ramírez LA, Ryu S (2013) Optogenetic elevation of endogenous glucocorticoid level in larval zebrafish. *Front Neural Circuits* 7:82.
41. Hartmann A, et al. (2013) Optogenetic modulation of an adenylate cyclase in Toxoplasma gondii demonstrates a requirement of the parasite cAMP for host-cell invasion and stage differentiation. *J Biol Chem* 288(19):13705–13717.
42. Wagner JR, et al. (2008) Mutational analysis of Deinococcus radiodurans bacteriophytochrome reveals key amino acids necessary for the photochromicity and proton exchange cycle of phytochromes. *J Biol Chem* 283(18):12212–12226.
43. Jaubert M, et al. (2007) A singular bacteriophytochrome acquired by lateral gene transfer. *J Biol Chem* 282(10):7320–7328.
44. Shimizu-Sato S, Huq E, Tepperman JM, Quail PH (2002) A light-switchable gene promoter system. *Nat Biotechnol* 20(10):1041–1044.
45. Piatkevich KD, Subach FV, Verkhusha VV (2013) Engineering of bacterial phytochromes for near-infrared imaging, sensing, and light-control in mammals. *Chem Soc Rev* 42(8):3441–3452.

Supporting Information

Gasser et al. 10.1073/pnas.1321600111

SI Materials and Methods

Molecular Biology. For expression in *Escherichia coli*, the DNA encoding residues 1–506 of *Deinococcus radiodurans* bacterial phytochrome (*Dr*BPhy; UniProt BPHY_DEIRA) was amplified by PCR from the *D. radiodurans* type strain DSM 20539 (DSMZ). The gene encoding residues 553–941 of *Homo sapiens* cAMP/cGMP-specific phosphodiesterase 2A (*Hs*PDE2A; UniProt PDE2A_HUMAN) was synthesized with *E. coli*-adapted codon use (Geneart). The fusion construct LAPD+2 between *Dr*BPhy (amino acids 1–506) and *Hs*PDE2A (amino acids 553–941) was generated by restriction cloning in the pET-28c vector (Novagen, Merck). Subcloning into the pASK43 vector (IBA GmbH) using NheI/HindIII furnished LAPD+2 with a C-terminal hexahistidine tag. Light-activated phosphodiesterase (LAPD), the C24A mutant of LAPD, and LAPD linker variants were generated by site-directed mutagenesis using the QuikChange protocol (Invitrogen, Life Technologies). For studies in eukaryotic cells, genes of *Dr*BPhy and *Hs*PDE2A with *H. sapiens*-adapted codon use were obtained by gene synthesis (Geneart) or by amplification from a full-length cDNA clone of *Hs*PDE2A (imaGenes GmbH), respectively. The LAPD fusion construct with *H. sapiens*-adapted codon use was constructed in pASK43 as described above. For expression in CHO cells, the LAPD gene was subcloned under the control of a CMV promoter in pEGFP-N1 (Clontech) using NheI/NotI, thereby removing the EGFP tag on the vector. For RNA production for zebrafish experiments, the LAPD gene was cloned into the pGEM vector (Promega). All constructs were confirmed by DNA sequencing (GATC Biotech).

Protein Expression and Purification. The pASK43 expression plasmids encoding LAPD variants were transformed into *E. coli* BL21 (DE3) cells carrying the pKT270 plasmid (1), which encodes *Synechocystis* sp. heme oxygenase 1. Five hundred milliliters of LB was inoculated and incubated at 37 °C and 225 rpm (New Brunswick Innova 43R incubator shaker); protein expression was induced at an OD at 600 nm of ∼0.5 by adding 0.2 $\mu g \cdot mL^{-1}$ anhydrotetracycline, 1 mM isopropyl-β-D-thiogalactopyranoside, and 500 μM δ-aminolevulinic acid hydrochloride. After incubation for 18 h at 16 °C and 225 rpm (New Brunswick Innova 43R incubator shaker), cells were harvested by centrifugation and suspended in lysis buffer [50 mM Tris·HCl (pH 8.0), 20 mM NaCl, 20 mM imidazole, Complete Ultra protease inhibitor mixture (Roche), lysozyme, DNaseI]. Upon lysis by sonication, the cleared lysate was incubated in the presence of 100 μM biliverdin hydrochloride (Frontier Scientific) and 5 mM Tris-(2-carboxyethyl)-phosphine hydrochloride for 1 h at 4 °C. Following incubation, the lysate was purified over a gravity-flow Co^{2+}-nitrilotriacetic acid affinity chromatography column (HisPur Cobalt Resin; Thermo Scientific). His-tagged protein was eluted with buffer containing 200 mM imidazole, dialyzed against storage buffer [20 mM Tris·HCl (pH 8.0), 20 mM NaCl, 5 mM β-mercaptoethanol], and concentrated with a centrifugal filter device (10,000-Da size cutoff; Corning). Purified samples were analyzed by gel electrophoresis, where protein was stained with Coomassie Brilliant Blue, and covalently bound biliverdin was monitored via zinc-induced fluorescence (2). Expression and purification were performed at 4 °C in the dark or under dim green light. Protein concentration was determined by absorption spectroscopy with an Agilent 8453 UV-visible spectrophotometer (Agilent Technologies) using an extinction coefficient of 45,700 $M^{-1} \cdot cm^{-1}$ at the isosbestic point (724 nm) (3). The degree of biliverdin incorporation was determined by absorption spectroscopy of LAPD denatured in 6.5 M guanidine hydrochloride (4). The amount of chromophore was calculated using the extinction coefficient for free biliverdin at 388 nm of 39,900 $M^{-1} \cdot cm^{-1}$; notably, the absorption of biliverdin at this wavelength is little affected by denaturant addition (4). The amount of protein was calculated based on absorption at 280 nm after correcting for the contribution of biliverdin absorption at this wavelength.

In Vitro Activity Assays. Catalytic activity was measured at 25 °C in solutions containing 5 nM enzyme (LAPD or variants), 50 mM Tris·HCl (pH 8.0), 8.3 mM $MgCl_2$, 50 $\mu g \cdot mL^{-1}$ BSA, and 7 mM β-mercaptoethanol (5). Reactions were started by adding 25–2,000 μM cAMP or cGMP. Experiments were conducted under dark conditions (i.e., dim green light) or under illumination 2 min before and during the reaction. A bandpass filter (ThorLabs) was used to select a wavelength of 690 nm (FWHM, 10 nm; power, 3.3 $mW \cdot cm^{-2}$) or light-emitting diodes of 455 nm (FWHM, 20 nm; power, 75 $mW \cdot cm^{-2}$) and 850 nm (FWHM, 30 nm; power, 28 $mW \cdot cm^{-2}$). For white-light irradiation, a tungsten halogen cold-light source was used (150 W, DCR III; Schott). Aliquots taken after 15 s to 2 min of reaction time were immediately transferred to 95 °C to stop the reaction and to denature the PDE enzyme. Samples were cleared by centrifugation and filtration (0.2-μm pore size, Chromafil; Macherey–Nagel), and were analyzed by HPLC (Knauer). cGMP and GMP were separated on a C18 reverse-phase column (Supelco; Sigma–Aldrich) using isocratic conditions [100 mM potassium phosphate (pH 5.9), 4 mM tetrabutylammonium iodide, 10% (vol/vol) methanol] (6). cAMP and AMP were separated on a C18 reverse-phase column using gradient elution [buffer A: 25 mM potassium phosphate (pH 5.5); buffer B: 94 mM potassium phosphate (pH 5.5); 25% (vol/vol) acetonitrile; gradient: 0–70% B within 12.5 min] (7). Elution was monitored by absorbance at 253 nm; data were evaluated with Clarity Chrom (Knauer) and Origin (Origin Lab Corp.). Peak areas were integrated and assigned to the educt cyclic NMP and the product NMP based on retention times of the corresponding standard compounds. To account for loading differences, we used an internal standardization procedure, where the product amount is normalized to the sum of the educt and product amounts.

In Vivo Activity Assays in CHO Cells. To generate a stable LAPD reporter cell line, a precursor atrial natriuretic peptide (ANP) reporter cell line (8) was cotransfected with a LAPD construct and the pcDNA3.1/hygro vector (Invitrogen). Stably transfected clones were obtained by hygromycin selection (0.4 $mg \cdot mL^{-1}$) and were characterized by ANP stimulation plus/minus illumination. One clonal cell line was selected for further experiments and is referred to as the LAPD reporter cell line. In parallel, a stable WT PDE2A reporter cell line was generated as before (9). Cultures of LAPD and PDE2A cell lines were grown in black 384-well microtiter plates (9). Following inoculation of ∼2,500 cells per well, the plates were incubated for 24 or 48 h at 37 °C and 5% (vol/vol) CO_2. Supernatant culture medium was discarded, and cells were loaded with 5 $\mu g \cdot mL^{-1}$ coelenterazine (CAS no. 55779-48-1; P. J. K. GmbH) in Ca^{2+}-free Tyrode solution [20 mM Hepes (pH 7.4), 130 mM NaCl, 5 mM KCl, 1 mM $MgCl_2$, 4.8 mM $NaHCO_3$] for 3 h at 37 °C and 5% (vol/vol) CO_2. ANP stimulation was performed in the absence or presence of the PDE2-specific inhibitor BAY 60-7550 (Axxora Life Sciences, Inc.). Both ANP and the inhibitor were dissolved in Ca^{2+}-free Tyrode solution containing 1 $mg \cdot mL^{-1}$ BSA. During incubation for 10 min, cells were either illuminated with white light (3,000

LX) or kept in the dark. Aequorin luminescence was measured immediately before and for 50 s following addition of Ca^{2+} ions to a final concentration of 3 mM using a CCD camera (Hamamatsu Corporation) in a light-tight box. The prism software (GraphPad Software, Inc.) was used for curve fitting and calculation of the EC_{50}, which are given as mean ± SEM (n = 6–7).

In Vivo Activity Assays in Zebrafish Embryos. Zebrafish husbandry and maintenance were carried out under standard conditions (10). All experiments performed in this study were conducted according to the guidelines of the German animal welfare law and were approved by the Animal Protection Office of the Max Planck Institute of Medical Research/University of Heidelberg. LAPD RNA was prepared from the pGEM-LAPD vector using the mMessage mMachine T7 Ultra Kit (Ambion), and 2 pg of this RNA was injected into WT (AB and TL zebrafish strains) embryos at the one-cell stage. Embryos were maintained in the dark and were dechorionated manually at 1 d postfertilization. Both uninjected controls and LAPD-injected embryos were treated with 300 μM forskolin and illuminated for 5 h with 625-nm light (1.1 $mW{\cdot}cm^{-2}$) or 950-nm light (270 $\mu W{\cdot}cm^{-2}$). Embryos were collected immediately afterward and instantly homogenized in 0.1 M hydrochloric acid. After centrifugation, the supernatants were stored at −20 °C. The cAMP levels were determined using a cAMP ELISA kit according to the manufacturer's protocol (Enzo Life Sciences); actual cAMP concentrations were calculated based on known cAMP standards.

Structural Analysis. Using LSQKAB (11), the structures of *Hs*PDE2A [Protein Data Bank (PDB) ID code 3IBJ (5)] and *Pseudomonas aeruginosa* bacterial phytochrome (*Pa*BPhy) [PDB ID code 3C2W (12)] were superposed with regard to their cGMP PDE/adenylyl cyclase/FhlA (GAF)-B– and phytochrome (PHY)-specific domains, respectively. The rotation matrix for this transformation is [[0.023, 0.446, −0.895], [0.247, −0.870, −0.427], [−0.969, −0.211, −0.130]], and the translation vector is [−59.5 Å, 30.2 Å, 105.8 Å]. Based on this superposition, a model of LAPD+2 was generated, where the orientation of the helices directly C-terminal of the *Pa*BPhy PHY domain was manually adjusted to achieve good overlap with the helices N-terminal of the *Hs*PDE2A catalytic domain. Molecule graphics were prepared with PyMOL (Schrödinger, LLC).

1. Mukougawa K, Kanamoto H, Kobayashi T, Yokota A, Kohchi T (2006) Metabolic engineering to produce phytochromes with phytochromobilin, phycocyanobilin, or phycoerythrobilin chromophore in Escherichia coli. *FEBS Lett* 580(5):1333–1338.
2. Berkelman TR, Lagarias JC (1986) Visualization of bilin-linked peptides and proteins in polyacrylamide gels. *Anal Biochem* 156(1):194–201.
3. Wagner JR, et al. (2008) Mutational analysis of Deinococcus radiodurans bacteriophytochrome reveals key amino acids necessary for the photochromicity and proton exchange cycle of phytochromes. *J Biol Chem* 283(18):12212–12226.
4. Shu X, et al. (2009) Mammalian expression of infrared fluorescent proteins engineered from a bacterial phytochrome. *Science* 324(5928):804–807.
5. Pandit J, Forman MD, Fennell KF, Dillman KS, Menniti FS (2009) Mechanism for the allosteric regulation of phosphodiesterase 2A deduced from the X-ray structure of a near full-length construct. *Proc Natl Acad Sci USA* 106(43):18225–18230.
6. Ryjenkov DA, Tarutina M, Moskvin OV, Gomelsky M (2005) Cyclic diguanylate is a ubiquitous signaling molecule in bacteria: Insights into biochemistry of the GGDEF protein domain. *J Bacteriol* 187(5):1792–1798.
7. Díaz Enrich MJ, Villamarín JA, Ramos Martínez JI, Ibarguren I (2000) Measurement of adenosine 3′,5′-cyclic monophosphate and guanosine 3′, 5′-cyclic monophosphate in mussel (Mytilus galloprovincialis lmk.) by high-performance liquid chromatography with diode array detection. *Anal Biochem* 285(1):105–112.
8. Wunder F, Woermann A, Geerts A, Milde M (2013) Pharmacological characterization of receptor guanylyl cyclase reporter cell lines. *Eur J Pharmacol* 698(1-3):131–136.
9. Wunder F, Gnoth MJ, Geerts A, Barufe D (2009) A novel PDE2A reporter cell line: Characterization of the cellular activity of PDE inhibitors. *Mol Pharm* 6(1):326–336.
10. Westerfield M (2000) *The Zebrafish Book: A Guide for the Laboratory Use of Zebrafish* (Danio rerio) (Univ of Oregon Press, Eugene, OR), 4th Ed.
11. Kabsch W (1976) A solution for the best rotation to relate two sets of vectors. *Acta Crystallogr A* 32:922–923.
12. Yang X, Kuk J, Moffat K (2008) Crystal structure of Pseudomonas aeruginosa bacteriophytochrome: Photoconversion and signal transduction. *Proc Natl Acad Sci USA* 105(38):14715–14720.

Fig. S1. Structure-based alignment of coiled-coil linkers in *Hs*PDE2A and BPhys. (*A*) Structure-based alignment of the coiled-coil linker region of *Pseudomonas aeruginosa* BPhP (*Pa*BPhP), *Deinococcus radiodurans BPhP (Dr*BPhP), and *Hs*PDE2A (compare Fig. 1*C*) provides design prescriptions for LAPD+2, whose sequence is indicated by the arrow. (*B*) The LAPD construct, variants LAPD−1 through LAPD−4 and variants LAPD+1 through LAPD+7 were obtained by consecutively deleting residues from the linker or by inserting residues into the linker (compare Table S1).

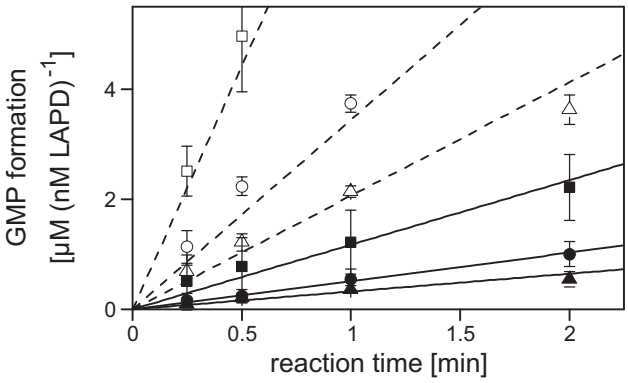

Fig. S2. Red-light–activated cGMP hydrolysis by LAPD illustrated in a magnified view of Fig. 2*B*. Integration of peak areas from HPLC analysis yields initial reaction velocities, v_0, at concentrations of 50 μM (▲), 100 μM (●), and 500 μM (■) cGMP. LAPD activity is enhanced under 690-nm light (open symbols) compared with dark conditions (closed symbols). Data are mean ± SD of two measurements; lines denote linear fits to determine v_0 values.

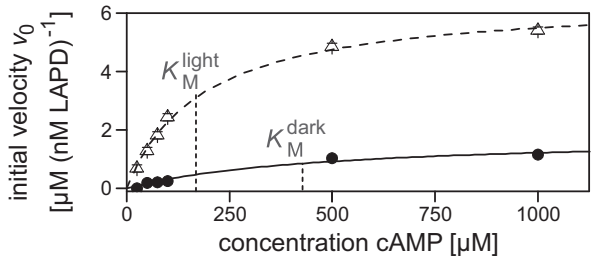

Fig. S3. Red-light–activated cAMP hydrolysis by LAPD. LAPD displays Michaelis–Menten kinetics for cAMP hydrolysis in both darkness (●, solid line) and under 690-nm light (Δ, dashed line). The v_0 values were determined by least-squares fitting and are reported as mean ± asymptotic SE. The maximum velocity, v_{max}, is increased from 1.8 ± 0.3 μM·min^{-1} (nM LAPD)$^{-1}$ in the dark to 6.5 ± 0.2 μM·min^{-1} (nM LAPD)$^{-1}$ under 690-nm light; the K_m value is decreased from 470 ± 170 μM in the dark to 180 ± 20 μM under 690-nm light. Lines denote fits to hyperbolic functions.

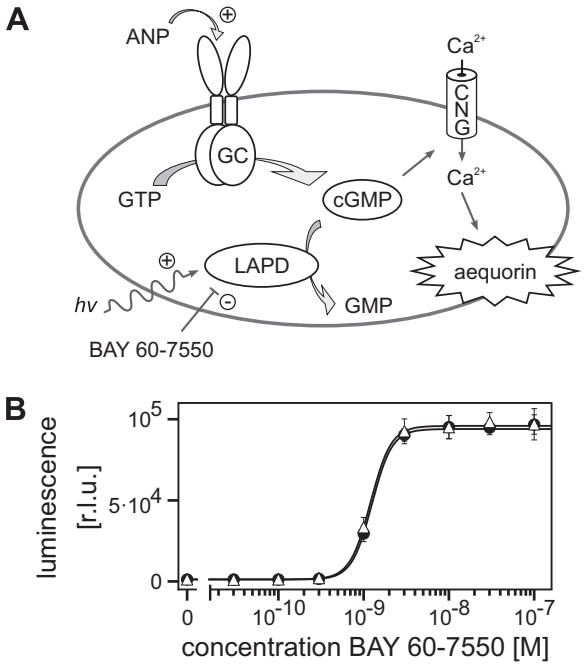

Fig. S4. CHO cells expressing WT *Hs*PDE2A do not respond to light. (*A*) Schematic of the LAPD reporter CHO cell line that constitutively expresses the ANP receptor and a cGMP-gated cyclic nucleotide–gated (CNG) channel. ANP addition triggers intracellular cGMP synthesis and opening of the CNG channel. Resultant calcium influx enhances luminescence of an aequorin reporter. Hydrolysis of cGMP by LAPD hence results in channel closing and decreased luminescence. (*B*) CHO cells stably transfected with WT *Hs*PDE2A instead of LAPD show no light dependence of PDE activity. Cells were stimulated with 10 nM ANP in the presence of different concentrations of the PDE2-specific inhibitor BAY 60-7550. Symbols denote reporter cell bioluminescence measured under dark (●) or light (Δ) conditions. Luminescence data are reported as relative light units (r.l.u.) and represent mean ± SEM of six to seven measurements; lines denote fits to hyperbolic functions.

Table S1. Fusion constructs between *Dr*BPhy and *Hs*PDE2A

	Residues from	
Construct	*Dr*BPhy	*Hs*PDE2A
LAPD−4	1–506	559–941
LAPD−3	1–506	558–941
LAPD−2	1–506	557–941
LAPD−1	1–506	556–941
LAPD	1–506	555–941
LAPD+1	1–506	554–941
LAPD+2	1–506	553–941
LAPD+3	1–507	553–941
LAPD+4	1–508	553–941
LAPD+5	1–509	553–941
LAPD+6	1–510	553–941
LAPD+7	1–511	553–941